Research Article

Jeong-Ki Kim, Rajkumar Bandi, Ramakrishna Dadigala, Song-Yi Han, Le Van Hai, Seung-Woo Cho, Seo-Young Ma, Da-Young Lee, Gu-Joong Kwon, and Seung-Hwan Lee*

Characteristics of cellulose nanofibril films prepared by liquid- and gas-phase esterification processes

https://doi.org/10.1515/epoly-2023-0093 received July 07, 2023; accepted December 10, 2023

Abstract: Cellulose nanofibrils (CNFs) are versatile materials, but their sensitivity to humidity affects performance. Esterification with fatty acids enhances the hydrophobicity of CNF films. This study compared gas- and liquid-phase esterification using three fatty acid chlorides at different dosages. Gas-phase esterification minimally affected cellulose crystallinity, maintaining a crystallinity index exceeding 55.8%, whereas liquid-phase esterification significantly reduced crystallinity. Gas-phase esterification achieved hydrophobicity (water contact angle >100°) with less fatty acid chlorides (0.50 eg/OH) compared to liquid-phase esterification (1.00 eg/ OH). Tensile strength significantly dropped in the liquid phase (68.4-6 MPa) and up to an 8-fold decrease in the elastic modulus. Conversely, gas-phase esterification maintained tensile strength over 40 MPa, and elastic modulus increased by a minimum of 2.5 times. However, gas-phase esterification resulted in a 5-fold reduction in elongation at break (%). Thermogravimetric analysis indicated a high T_{max} of 362°C for liquid-phase esterified samples and a substantial 24.9% residual weight for gas-phase esterified samples.

Environmental Sciences, Kangwon National University, Chuncheon 24341, Republic of Korea

Paikumar Randi, Pamakrichna Dadigala, Song Vi Han, Le Van Hai

Rajkumar Bandi, Ramakrishna Dadigala, Song-Yi Han, Le Van Hai, Gu-Joong Kwon: Institute of Forest Science, Kangwon National University, Chuncheon 24341, Republic of Korea **Keywords:** nanocellulose, fatty acid chlorides, hydrophobicity, tensile properties, crystallinity

1 Introduction

Cellulose nanofibrils (CNFs) are fibrous nanomaterials derived from cellulose through mechanical separation, often involving a chemical pretreatment (1-3). The unique characteristics of CNFs, such as their ability to form porous entangled networks and their nanoscale dimensions, make them ideal materials for the production of membranes, films, and nanopapers (4). CNF films exhibit a range of desirable properties, including optical, thermal, mechanical, and barrier properties (5,6). Moreover, their biodegradability and renewability make them attractive alternatives to petroleum-based plastics and a potential next-generation high-performance material (7,8). Several manufacturing methods can be employed to produce CNF films, such as solution casting, spin coating, and layer-by-layer assembly (9,10). Because of their versatility, CNF films have applications in various fields, including packaging (11–13), supercapacitor (14), EMI shielding (15), solar evaporators (16), uranium(vi) capture (17), and dye purification (18).

However, a limitation of CNF films is their susceptibility to humidity. The adsorption of water molecules on the surface of the CNF films disrupts the hydrogen bonding between the CNFs. Consequently, as relative humidity increases, the mechanical strength, thermal diffusivity, and barrier properties of CNF films tend to diminish (19–21). Therefore, enhancing the hydrophobicity of CNF films is crucial for their use in highly humid environments. Esterification of CNFs using fatty acid chlorides involves the substitution of the hydroxyl groups of CNFs with fatty acids through ester bonds. Hydrophobicity is achieved by replacing the hydroxyl groups with long carbon chains from fatty acids, which leads to improved dispersibility

^{*} Corresponding author: Seung-Hwan Lee, Department of Forest Biomaterials Engineering, College of Forest and Environmental Sciences, Kangwon National University, Chuncheon 24341, Republic of Korea; Institute of Forest Science, Kangwon National University, Chuncheon 24341, Republic of Korea, e-mail: Ishyhk@kangwon.ac.kr

Jeong-Ki Kim, Seung-Woo Cho, Seo-Young Ma, Da-Young Lee:

Department of Forest Biomaterials Engineering, College of Forest and

in nonpolar solvents and enhanced interfacial adhesion with hydrophobic polymers. Esterification typically involves the addition of fatty acid chlorides to the CNFs dispersed in a solvent. This liquid-phase esterification occurred throughout the cellulose structure, ensuring good reactivity. However, substituting the hydroxyl groups with fatty acids reduces the number of intramolecular and intermolecular hydrogen bonds in cellulose, which can weaken the strength of the cellulose. In contrast, gasphase esterification involves vaporizing fatty acid chlorides at high temperatures, allowing CNFs to react with the gaseous fatty acid chlorides (22,23). This method selectively reacts only at accessible regions, preserving the crystallinity and hydrogen bonding in the CNF film core. However, gas-phase esterification of CNF films, to the best of our knowledge, has not been studied yet. Previous studies have primarily focused on the gas-phase esterification of CNF powder samples or aerogels. Rodionova et al. reported gas-phase esterification of microfibrillated cellulose films and examined their barrier properties (23). Based on these findings, we hypothesized that the gasphase esterification of CNF films could yield hydrophobic films with satisfactory mechanical properties, making them suitable for a wide range of applications.

In this study, we propose gas-phase esterification of CNF films and compare it with liquid-phase esterification. Three types of fatty acid chlorides (octanoyl, lauroyl, and palmitoyl chlorides) were employed at four different dosages (0.50, 0.66, 1.00, and 2.00 eq/cellulose OH). The films were characterized using Fourier-transform infrared spectroscopy (FTIR) and X-ray diffraction (XRD). The water contact angles, tensile properties, and thermal stability were also investigated (Scheme 1).

2 Materials and methods

2.1 Materials

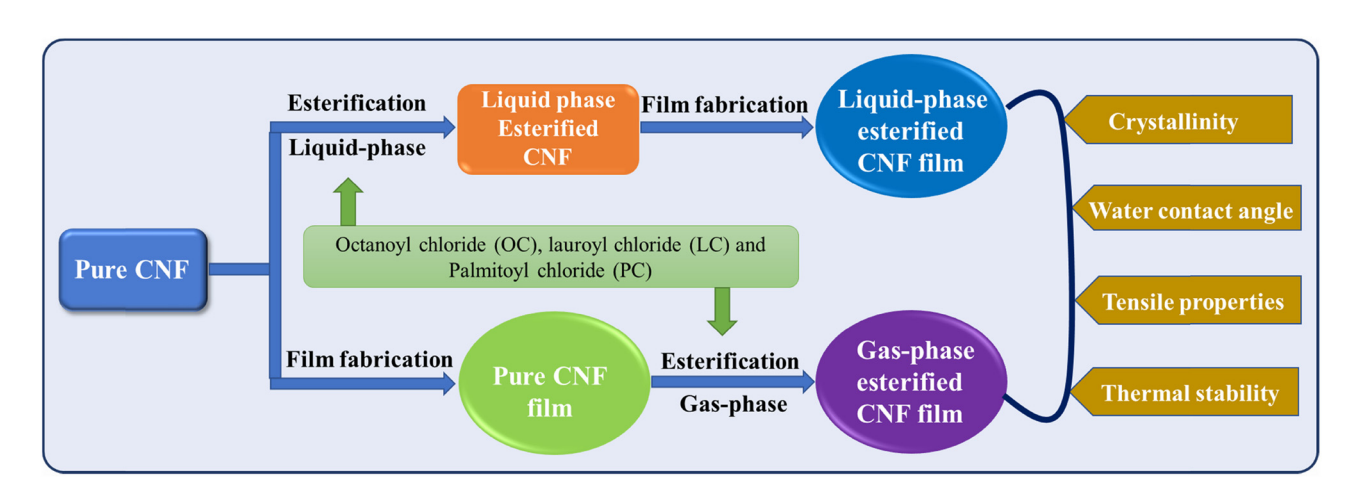
CNF aqueous dispersion was obtained from Cellulose Lab Co., Ltd. (QC, Canada). Octanoyl chloride (OC), lauroyl chloride (LC), and palmitoyl chloride (PC) (TCI Co., Japan; >98.0%) were used to esterify the CNFs. Pyridine (>99.5%), *N,N*-dimethylformamide (DMF, >99.5%), and chloroform (>99.5%) were obtained from Daejung Chemical & Metals Co., Ltd. (Republic of Korea).

2.2 Liquid-phase esterification of CNFs

CNF aqueous dispersion was solvent-exchanged with DMF, and 100 g of 1 wt% DMF dispersion (CNF dry weight: 1 g and total hydroxyl groups: 18.51 mmol·g⁻¹) was prepared. The solvent exchange was performed via repeated centrifugation and redispersion. Fatty acid chloride (0.5, 0.66 1.0, and 2.0 eq/cellulose OH) and pyridine (2.0 eq/cellulose OH) were added under a nitrogen atmosphere. Then, they were allowed to react at 80°C for 6 h and the reaction was terminated by adding excess ethanol. CNFs were washed with ethanol via vacuum filtration. The esterified CNFs (eCNFs) were dispersed and stored in chloroform to prepare eCNF films.

2.3 Preparation of pure CNF and the eCNF film

Pure CNFs and eCNFs were dispersed in 200 g of water and chloroform, respectively, at a concentration of 0.1 wt%. The



Scheme 1: Schematic illustration showing the gas- and liquid-phase esterification of CNF and its characterization.

suspensions were sonicated for 1 min in an ultrasonicator (VCX130PBS; Sonics & Materials, Inc., USA) and vacuumfiltered through a silicone-coated membrane filter. The films were then prepared by hot pressing at 105°C for 10 min under a pressure of 15 MPa.

2.4 Gas-phase esterification of the pure CNF film

A general gas-phase esterification method was employed in this study. A graphical representation of the reaction setup is shown in Figure 1. Fatty acid chloride was placed at the bottom of the reaction vessel, and a pure CNF film was placed on a PTFE mesh positioned 15 cm above the fatty acid chloride. The reaction vessel was sealed and connected to a vacuum pump on one side and a nitrogen gas inlet on the other side. The esterification reaction was performed at 150°C for 1 h at a pressure of 50 mbar under a continuous nitrogen flow.

2.5 FTIR spectroscopy

The FTIR spectra of the pure CNF and eCNF films were recorded using an FTIR instrument (Nicolet Summit, Thermo Fisher Scientific, USA). A total of 32 scans were performed for each sample in the range of 4,000–500 cm⁻¹.

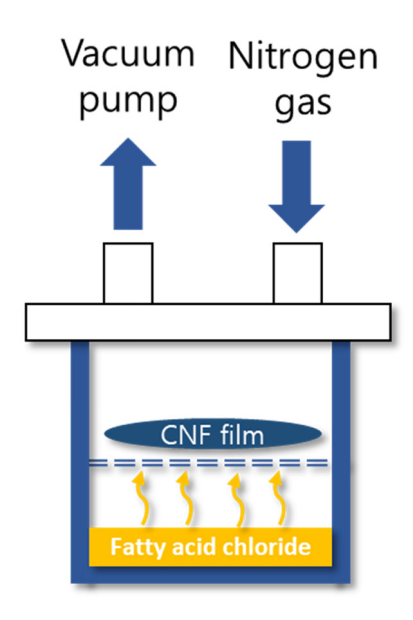


Figure 1: Graphical representation of apparatus used for gas-phase esterification.

2.6 XRD spectroscopy

The XRD patterns were recorded on an X-ray diffractometer (X'Pert PRO MPD PANalytical, Netherlands) in a 2θ range of 10–35°. The crystallinity index (CrI) was calculated using the following equation (the Segal method):

Crystallinity index (Crl, %) =
$$\frac{I_{200} - I_{am}}{I_{200}} \times 100$$
 (1)

where I_{002} and I_{am} are the intensities at $2\theta = 22.7^{\circ}$ and 18° , which represent crystalline and amorphous states, respectively.

2.7 Contact angle analysis

The static sessile-drop method was used to determine the water contact angles of the pure CNF and eCNF films using a contact angle analyzer (Theta Lite, Biolin Scientific, UK). The measurements were conducted at room temperature (22–25°C). A 5 µL droplet was placed on the film, and the drop image was processed using an image analysis system.

2.8 Scanning electron microscopic (SEM) analysis

The morphologies of pure CNF and eCNF films were studied by SEM (S-4800, Hitachi, Ltd., Japan). Prior to observation, the films were placed on aluminum stubs, and coated with iridium using a sputter coater (EMACE600, Leica Microsystems, Ltd., Wetzlar, Germany). The morphologies were observed at an accelerating voltage of 1 kV.

2.9 Tensile properties

The tensile properties were measured using a universal testing machine (TO-102D, Test One, Republic of Korea) at a crosshead speed of 10 mm·min⁻¹ with a specimen span length of 30 mm. The samples were cut to dimensions of $50 \text{ mm} \times 10 \text{ mm}$ (length \times width). At least five specimens were tested for each sample, and the results were averaged. Before the measurement, samples were maintained in a thermohygrostat at 25°C and a relative humidity of 40% to standardize the effect of relative humidity on the tensile properties.

2.10 Thermogravimetric analysis (TGA)

TGA of pure CNF and eCNF films was performed using a thermogravimetric analyzer (SDT Q600; TA Instruments, New Castle, DE, USA). The temperature was controlled from 30°C to 600°C at a heating rate of 10°C·min⁻¹. A high purity nitrogen stream with a rate of 100 mL·min⁻¹ was continuously passed into the furnace to prevent any unwanted oxidation.

3 Results and discussion

3.1 FTIR spectroscopy

FTIR analysis was performed to confirm the chemical modification of the CNFs by esterification. The FTIR spectra of the pure CNF and eCNF films esterified by gas- and liquidphase esterification are shown in Figure 2. The FTIR spectrum of pure CNFs exhibited characteristic peaks corresponding to the cellulose structure. Three major changes were observed after esterification. A new peak evolved at 1,740 cm⁻¹, corresponding to the carbonyl stretching of the ester group. This confirmed the esterification reaction between the hydroxyl groups of cellulose and the acid chloride groups of the fatty acids. The second new peak was recorded in the range of 2,800-3,000 cm⁻¹, corresponding to the methylene groups (C-H) of fatty-acid side chains, and confirmed the grafting of the fatty acid to the CNF. As the amount of fatty acids increased, the intensities of the methylene and carbonyl signals increased. PC, with the longest side chain, exhibited high-intensity peaks in the 2,800–3,000 cm⁻¹ region. Additionally, a decrease in the intensity of the broadband at approximately 3,200–3,500 cm⁻¹, assigned to the O-H vibration in cellulose, suggested the consumption of hydroxyl groups in the esterification reaction (24).

The degree of substitution (DS) was calculated from the ratio of the FTIR peak intensities $I_{1,740}/I_{1,031}$, where $I_{1.740}$ and $I_{1.031}$ are the intensities of the C=0 stretching band and C-O stretching vibration of the cellulose backbone, respectively (25). As shown in Table 1, in the case of liquid-phase esterification, the DS increased significantly with an increase in the amount of fatty acid chloride. However, no such trend was observed for the gas-phase esterification. Here, a high DS was achieved even at low addition amounts, with no significant increase in the DS at high addition amounts. This difference can be ascribed to the distinct behaviors exhibited by the liquid- and gas-phase reactions. In the liquid phase, the esterification reaction occurs uniformly throughout the CNF surface, whereas in the gas phase, the reaction is concentrated on the film surface, with minimal or no reaction occurring within the interior of the CNF film.

3.2 XRD analysis

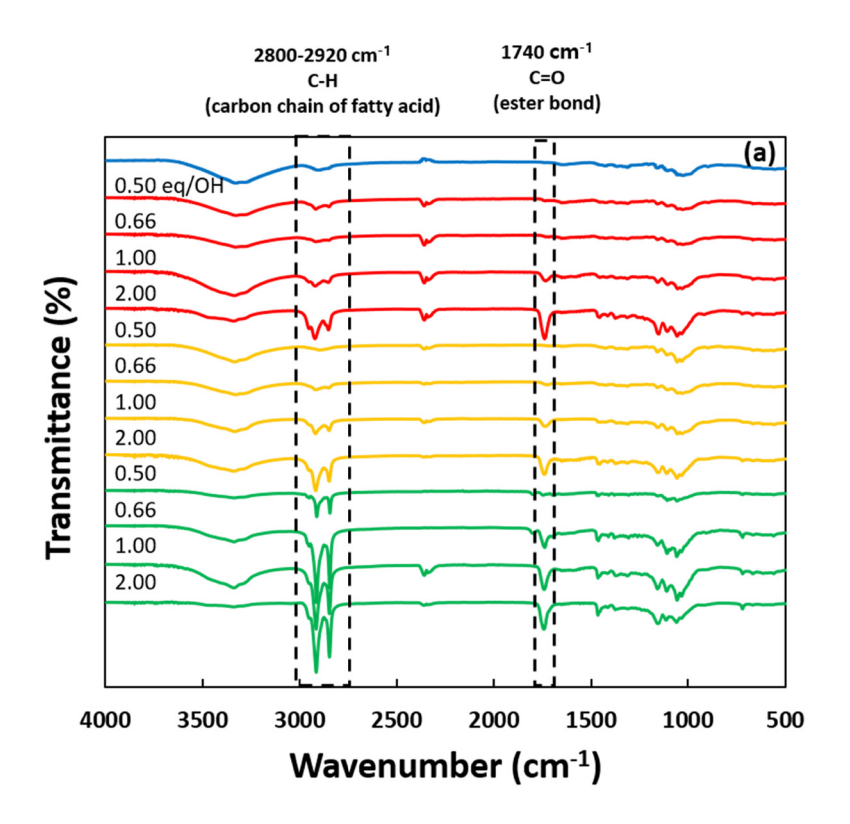
XRD was performed to investigate the effect of esterification on the crystalline structure of cellulose. As shown in Figure 3, the crystal structure of cellulose is strongly affected by liquid-phase esterification. The characteristic cellulose I peak intensities at 22° and 16.7° decreased with an increase in the amounts of fatty-acid chlorides added. Among the three fatty acid chlorides, PC, which has a long side chain, has a significant influence on the crystal structure. In the case of esterification with OC and LC, the cellulose crystal structure was maintained at low added amounts (0.50 and 0.66 eq/OH), whereas in the case of PC, it was destroyed at all equivalents. These observations are in good agreement with previous reports (26).

In contrast, the crystal structure of cellulose was mostly unaffected by gas-phase esterification. Except for small changes in the peak positions, characteristic cellulose I peaks were observed under all conditions. This difference between gas- and liquid-phase esterification can be ascribed to the limited access of fatty acid chloride molecules in the gas phase compared to those in the liquid phase. Vaporized fatty acid chloride molecules can react only on the surface of the film, leaving the core intact, thereby preserving its crystalline structure (22,27).

Table 2 lists the crystallinity indices of the CNF films, which were calculated using the ratio of the intensity of the crystalline peak to that of the amorphous peak obtained from the XRD patterns (the Segal method). The crystallinity index of the pure CNF film was 70.1%, which decreased after esterification. In general, the crystallinity index decreases with an increase in the degree of cellulose ester substitution (28). This phenomenon is evident in liquid-phase esterification. The introduction of fatty acids reduces the number of inter- and intra-molecular hydrogen bonds in cellulose, which in turn decreases its crystallinity (29). Gasphase esterification has less effect on crystallinity, suggesting that most of the reaction occurs on the film surface without modifying the core (30).

3.3 Contact angle analysis

Water contact angle measurements are an effective technique for assessing the hydrophobicity of a material. Figure 4 shows the variation in the water contact angles of the liquid- and gas-phase-eCNF films with the loading amounts of fatty acid chlorides. The pure CNF film exhibited a contact angle of 59°, indicating hydrophilicity. In the case of liquid-phase esterification, the contact angle increased with an increase in the



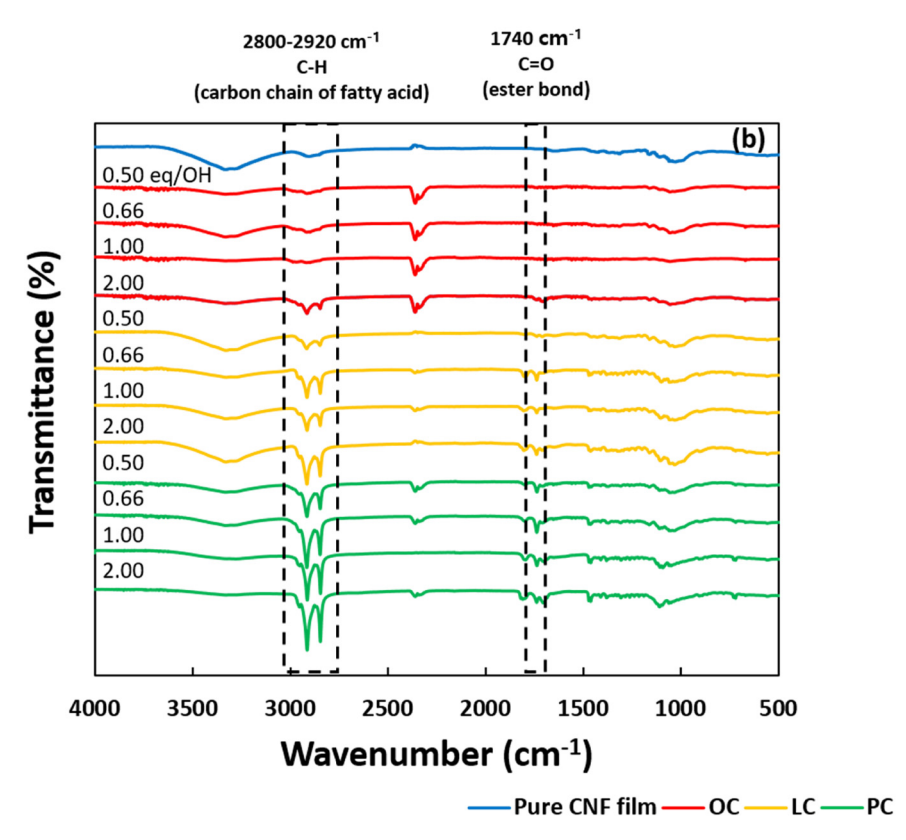


Figure 2: FTIR spectra of pure CNF and eCNF films obtained from (a) liquid-phase and (b) gas-phase esterifications for different amounts of fatty-acid chloride added.

Table 1: Degree of substitution in eCNF films

Esterification phase	Type of fatty acid chloride	Added amounts (eq/OH)	Degree of substitution
Liquid	ОС	0.50	0.20
		0.66	0.25
		1.00	0.53
		2.00	1.19
	LC	0.50	0.16
		0.66	0.24
		1.00	0.53
		2.00	0.96
	PC	0.50	0.43
		0.66	0.79
		1.00	1.20
		2.00	1.60
Gas	OC	0.50	0.48
		0.66	0.72
		1.00	0.80
		2.00	0.52
	LC	0.50	0.29
		0.66	0.47
		1.00	0.41
		2.00	0.49
	PC	0.50	0.64
		0.66	0.88
		1.00	0.98
		2.00	1.00

amount of added fatty acid chlorides. Hydrophobicity was not imparted at low loading amounts of 0.50 and 0.66 eq/OH (except for PC). At each added amount, the PC with the longest

side chain exhibited the highest contact angle, and a maximum value of 122° was observed at a high loading amount (2 eq/OH). In the case of gas-phase esterification, hydrophobicity was achieved even at a low fatty acid content, and no significant increase in the contact angle was observed with a further increase in the amount of fatty acid added. This is because, in the liquid-phase reaction, the fatty acid chloride reacts uniformly throughout the CNF film, whereas in the gas phase, it predominantly reacts on the surface.

It is well-established that water contact angle values can be affected not only by chemical functionalities but also by surface roughness. To investigate the impact of surface roughness on water contact angle values, we examined the surface morphologies of both pure CNF and eCNF films, which were derived from gas- and liquid-phase esterification processes. We focused our analysis on samples esterified with LC as representative cases for this study. Figure S1 illustrates that there is no substantial distinction in surface roughness between the pure CNF and eCNF films. Moreover, there is minimal differentiation between liquid- and gas-phase esterification methods, as well as variations in the quantity of LC (0.5 eq/OH and 2.0 eq/OH). These findings validate that the enhanced water contact angles can be attributed exclusively to the chemical modification involving long-chain fatty acids.

3.4 Tensile properties

The tensile strength, elastic modulus, and elongation at break were analyzed for the pure CNF and eCNF films to

(b)

Pure CNF film

OC

LC

35

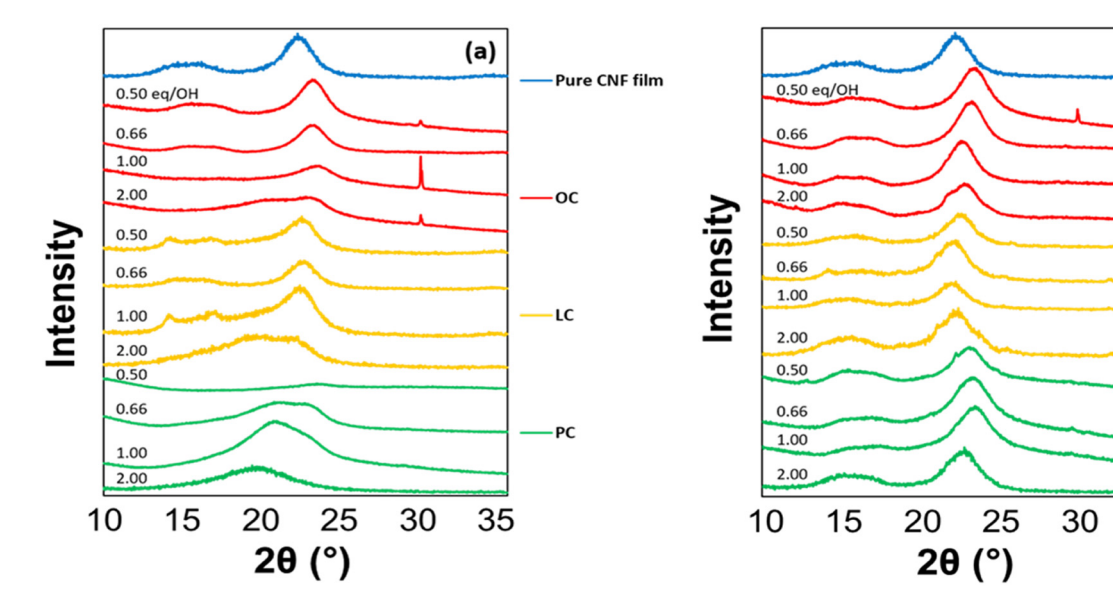


Figure 3: XRD patterns of pure CNF and eCNF films obtained from (a) liquid-phase and (b) gas-phase esterifications for different amounts of fatty-acid chlorides added.

Table 2: Crystallinity index of pure CNF and eCNF films

Esterification phase	Type of fatty acid chloride	Added amounts (eq/OH)	Crystallinity index (%)
Liquid	OC	0.50	69.4
		0.66	67.2
		1.00	Unable to measure
		2.00	Unable to measure
	LC	0.50	68.5
		0.66	67.8
		1.00	Unable to measure
		2.00	Unable to measure
	PC	0.50	Unable to measure
		0.66	Unable to measure
		1.00	Unable to measure
		2.00	Unable to measure
Gas	ОС	0.50	59.4
		0.66	55.8
		1.00	60.4
		2.00	58.9
	LC	0.50	63.8
		0.66	61.4
		1.00	60.0
		2.00	63.5
	PC	0.50	67.3
		0.66	60.0
		1.00	64.4
		2.00	67.1

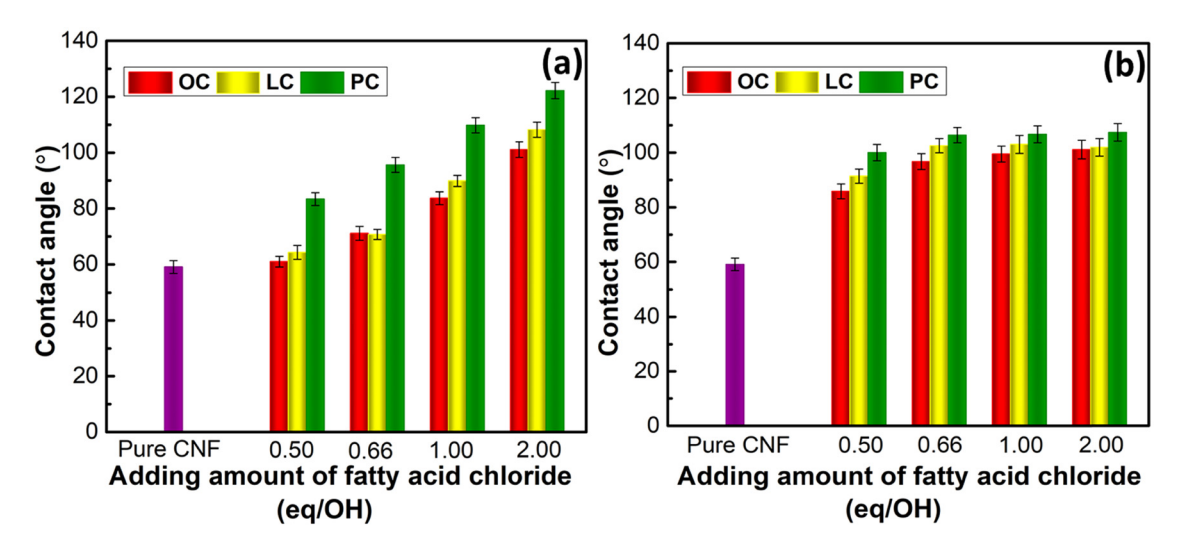


Figure 4: Water contact angles of pure CNF and eCNF films obtained from (a) liquid-phase and (b) gas-phase esterifications for different amounts of fatty-acid chlorides added.

investigate the impact of liquid- and gas-phase esterifications (Figure 5). For liquid-phase esterification, the tensile strength and elastic modulus decreased with an increase in the amount of added fatty acid chloride. This trend was observed for all three fatty acids; OC, with the shortest side chain, exhibited the highest values, and PC, with the longest side chain, exhibited the lowest values at each

added amount. This correlation agrees with the crystallinity index obtained from XRD, suggesting that the substantial decrease in tensile strength and elastic modulus may be attributed to changes in crystallinity. Additionally, the grafting of fatty acids onto CNFs can disrupt the intermolecular and intramolecular hydrogen bonds, further contributing to a reduction in strength.

8 — Jeong-Ki Kim et al. DE GRUYTER

Conversely, in the case of gas-phase esterification, no such trend was observed, and only a slight decrease in the tensile strength was recorded, even with high amounts of fatty acid chlorides. This phenomenon can be explained by the fact that the vaporized fatty acid chlorides react only with the surface of the CNF film, leaving the crystallinity and hydrogen bonds inside the film intact. In addition, after gas-phase esterification, the elastic modulus increased significantly,

and the elongation decreased sharply. Gas-phase eCNF films demonstrate a higher elastic modulus but a lower elongation-at-break when compared to liquid-phase eCNF films. This suggests that the gas-phase eCNF films exhibit a more brittle behavior, whereas the lower CrI in the liquid-phase eCNF films corresponds to a more ductile behavior, leading to increased elongation-at-break and a decreased elastic modulus. The brittleness of gas-phase eCNF films may also be attributed to the

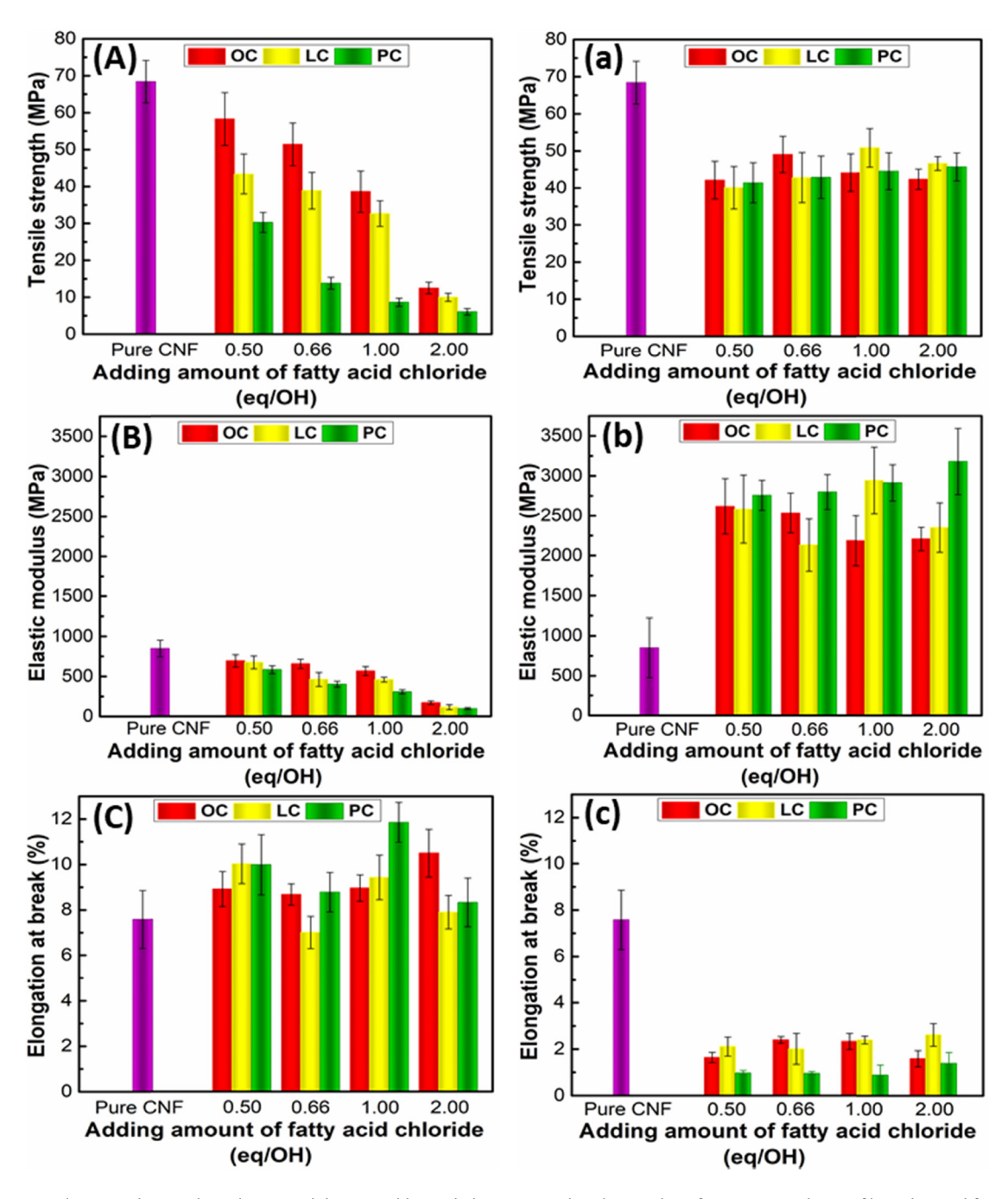


Figure 5: Tensile strength (A and a), elastic modulus (B and b), and elongation at break (C and c) of pure CNF and eCNF films obtained from liquid-phase (A, B, and C) and gas-phase (a, b, and c) esterifications for different amounts of fatty-acid chlorides added.

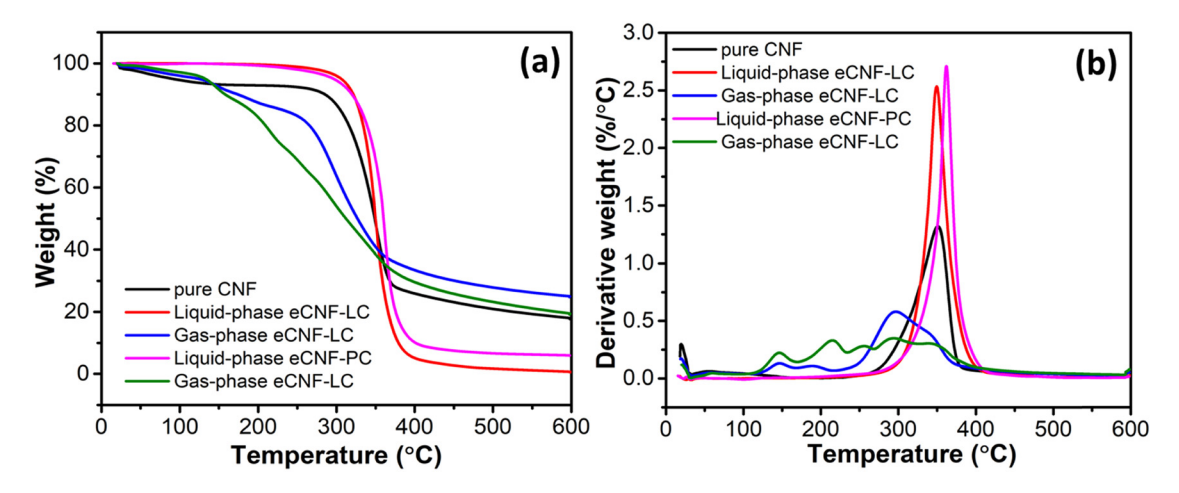


Figure 6: (a) TGA and (b) DTG curves of pure CNF and eCNFs prepared under different conditions (Note: the amount of fatty acid chloride added is 2.00 eq/OH).

Table 3: The maximal weight loss temperature ($T_{\rm max}$) and residual content at 600°C of TG and DTG analysis of pure CNF and eCNFs prepared under different conditions (Note: the added amount of fatty acid chloride is 2.00 eq/OH)

Sample	T _{max} (°C)	Residual weight (%)
Pure CNF	351	17.8
Liquid-phase eCNF-LC	349	0.6
Liquid-phase eCNF-PC	362	5.9
Gas-phase eCNF-LC	297	24.9
Gas-phase eCNF-PC	294	19.4

formation of HCl gas during the esterification process, which might cause some depolymerization of the cellulose molecules.

3.5 Thermal stability

TGA analysis of pure CNF and eCNF films was performed to study the effect of gas- and liquid-phase esterification on the thermal stability of pure CNFs. The TGA and DTG (derivative thermogravimetric) curves are depicted in Figure 6, while detailed thermal parameters, including $T_{\rm max}$ (the temperature at which maximum decomposition occurs) and the residual weight percentage, are listed in Table 3.

For the liquid-phase esterified samples, the $T_{\rm max}$ values are comparable to those of pure CNFs. However, there is a significant reduction in residual weight at 600°C. A single weight loss stage is observed in the samples, likely due to the substitution of most of the –OH groups responsible for CNF dehydration degradation. Consequently, a single phase of depolymerization involving both the CNF and the aliphatic chain of the fatty acid may have taken place (31). The lower

residual weight is likely attributed to the amorphous nature of eCNFs, which burned away without leaving char. Here, eCNF-PC demonstrated enhanced thermal stability when compared to eCNF-LC, as evidenced by higher $T_{\rm max}$ and greater residual weight values, possibly due to its high DS value, as observed in a previous study with CNC (31).

On the other hand, gas-phase esterification resulted in a substantial decrease in $T_{\rm max}$, and multiple weight loss stages were observed. This degradation pattern can be attributed to surface-only esterification and the production of HCl gas during the process. The presence of HCl gas may have locally depolymerized the CNF film on the surface. The loss of these smaller units, along with fatty acid side chains, likely contributed to the observed weight loss stages. Additionally, the high residual weight in gas-phase esterified samples can be associated with the retention of crystalline characteristics. As shown in Tables 2 and 3, eCNF-LC with a higher CrI than eCNF-PC exhibited a high residual weight. It is possible that the crystalline part remained as char during the thermal analysis.

All these findings indicate the reduced thermal stability of CNFs after esterification, which can be ascribed to the introduction of less stable side chains (32). Furthermore, the substantial disruption of the crystalline structure of cellulose during the esterification reaction makes derivatives with looser and disordered crystalline structures more susceptible to thermal decomposition.

4 Conclusions

This study compared the effects of liquid- and gas-phase esterification on the characteristics of CNF films. OC, LC,

and PC with different side-chain lengths were used in different dosages for esterification. Cellulose esterification was confirmed by detecting characteristic peaks in the FTIR spectra of the eCNF films related to fatty-acid chains and ester bonds. The DS analysis revealed that liquid-phase esterification resulted in higher levels of substitution at higher adding amounts of fatty-acid chloride, whereas gasphase esterification showed higher substitution at lower adding amounts. XRD analyses revealed that gas-phase esterification had a minimal impact on cellulose crystallinity, whereas liquid-phase esterification remarkably decreased the crystallinity. Water contact angle measurements revealed that gas-phase esterification achieved hydrophobicity with a smaller amount of fatty-acid chloride than liquid-phase esterification. Liquid-phase esterification deteriorated the tensile properties of the films, whereas gas-phase esterification allowed hydrophobization without substantial degradation of the tensile properties. In summary, this study highlights the advantages of gas-phase esterification over liquid-phase esterification in terms of maintaining cellulose crystallinity, achieving hydrophobicity with a smaller amount of fatty acid chloride, and preserving the tensile properties of the CNF films.

Funding information: This research was supported by the Basic Science Research Program through the National Research Foundation of Korea (NRF), funded by the Ministry of Education (No. 2018R1A6A1A03025582; No. 2021R1A2C2004941).

Author contributions: Jeong-Ki Kim: conceptualization, methodology, investigation, and writing – original draft; Rajkumar Bandi: conceptualization, methodology, and writing – review and editing; Ramakrishna Dadigala: data curation and visualization; Song-Yi Han: software and project administration; Le Van Hai: validation; Seung-Woo Cho: resources and formal analysis; Seo-Young Ma: resources; Da-Young Lee: data curation; Goo-Jung Kwon: conceptualization, methodology, and software; Seung-Hwan Lee: writing – review and editing, funding acquisition, and project administration.

Conflict of interest: Authors state no conflict of interest.

References

 Si R, Pu J, Luo H, Wu C, Duan G. Nanocellulose-based adsorbents for heavy metal ion. Polymers. 2022;14(24):5479. doi: 10.3390/ polym14245479.

- (2) Chen Y, Zhang L, Yang Y, Pang B, Xu W, Duan G, et al. Recent progress on nanocellulose aerogels: preparation, modification, composite fabrication, applications. Adv Mater. 2021;33(11):2005569. doi: 10.1002/adma.202005569.
- (3) Yan W, Liu J, Zheng X, Zhang J, Tang K. Wood-derived high-performance cellulose structural materials. E-Polymers. 2023;23(1):20230010. doi: 10.1515/epoly-2023-0010.
- (4) Rajala S, Siponkoski T, Sarlin E, Mettänen M, Vuoriluoto M, Pammo A, et al. Cellulose nanofibril film as a piezoelectric sensor material. ACS Appl Mater Interfaces. 2016;8(24):15607–14. doi: 10. 1021/acsami.6b03597.
- (5) Nogi M, Iwamoto S, Nakagaito AN, Yano H. Optically transparent nanofiber paper. Adv Mater. 2009;21(16):1595–8. doi: 10.1002/ adma.200803174.
- (6) Lavoine N, Desloges I, Dufresne A, Bras J. Microfibrillated cellulose – Its barrier properties and applications in cellulosic materials: A review. Carbohydr Polym. 2012;90(2):735–64. doi: 10.1016/j.carbpol. 2012.05.026.
- (7) Alavi M. Modifications of microcrystalline cellulose (MCC), nanofibrillated cellulose (NFC), and nanocrystalline cellulose (NCC) for antimicrobial and wound healing applications. E-Polymers. 2019;19(1):103–19. doi: 10.1515/epoly-2019-0013.
- (8) Hayajneh MT, Al-Shrida MM, Al-Oqla FM. Mechanical, thermal, and tribological characterization of bio-polymeric composites: A comprehensive review. E-Polymers. 2022;22(1):641–63. doi: 10.1515/ epoly-2022-0062.
- (9) Raghuwanshi VS, Garnier G. Cellulose nano-films as bio-interfaces. Front Chem. 2019;7:535. doi: 10.3389/fchem.2019.00535.
- (10) Wågberg L, Erlandsson J. The use of layer-by-layer self-assembly and nanocellulose to prepare advanced functional materials. Adv Mater. 2021;33(28):2001474. doi: 10.1002/adma.202001474.
- (11) Amoroso L, De France KJ, Milz CI, Siqueira G, Zimmermann T, Nyström G. Sustainable cellulose nanofiber films from carrot pomace as sprayable coatings for food packaging applications. ACS Sustain Chem Eng. 2022;10(1):342–52. doi: 10.1021/acssuschemeng. 1c06345.
- (12) Deng Z, Jung J, Zhao Y. Development, characterization, and validation of chitosan adsorbed cellulose nanofiber (CNF) films as water resistant and antibacterial food contact packaging. LWT. 2017;83:132–40. doi: 10.1016/j.lwt.2017.05.013.
- (13) Wang J, Han X, Zhang C, Liu K, Duan G, Wang J, et al. Source of nanocellulose and its application in nanocomposite packaging material: a review. Nanomaterials. 2022;12(18):3158. doi: 10.3390/ nano12183158.
- (14) Xiao J, Li H, Zhang H, He S, Zhang Q, Liu K, et al. Nanocellulose and its derived composite electrodes toward supercapacitors: Fabrication, properties, and challenges. J Bioresour Bioprod. 2022;7(4):245–69. doi: 10.1016/j.jobab.2022.05.003.
- (15) Chen Y, Pang L, Li Y, Luo H, Duan G, Mei C, et al. Ultra-thin and highly flexible cellulose nanofiber/silver nanowire conductive paper for effective electromagnetic interference shielding. Compos – A: Appl Sci Manuf. 2020;135:105960. doi: 10.1016/j.compositesa. 2020.105960.
- (16) Wu W, Xu Y, Ma X, Tian Z, Zhang C, Han J, et al. Cellulose-based interfacial solar evaporators: structural regulation and performance manipulation. Adv Funct Mater. 2023;33(36):2302351. doi: 10.1002/adfm.202302351.
- (17) Gao J, Yuan Y, Yu Q, Yan B, Qian Y, Wen J, et al. Bio-inspired antibacterial cellulose paper–poly(amidoxime) composite hydrogel for

- highly efficient uranium(VI) capture from seawater. Chem Commun. 2020;56(28):3935–8. doi: 2020/cc/c9cc09936k.
- (18) Chen Y, Li S, Li X, Mei C, Zheng J, Shiju E, et al. Liquid transport and real-time dye purification via lotus petiole-inspired long-rangeordered anisotropic cellulose nanofibril aerogels. ACS Nano. 2021;15(12):20666–77. doi: 10.1021/acsnano.1c10093.
- (19) Benítez AJ, Torres-Rendon J, Poutanen M, Walther A. Humidity and multiscale structure govern mechanical properties and deformation modes in films of native cellulose nanofibrils. Biomacromolecules. 2013;14(12):4497–506. doi: 10.1021/ bm401451m.
- (20) Izakura S, Koga H, Uetani K. Humidity-responsive thermal conduction properties of bacterial cellulose films. Cellulose. 2021;28(9):5363–72. doi: 10.1007/s10570-021-03888-6.
- (21) Wang J, Gardner DJ, Stark NM, Bousfield DW, Tajvidi M, Cai Z. Moisture and oxygen barrier properties of cellulose nanomaterial-based films. ACS Sustain Chem Eng. 2018;6(1):49–70. doi: 10.1021/acssuschemeng.7b03523.
- (22) Berlioz S, SMolina-Boisseau S, Nishiyama Y, Heux L. Gas-phase surface esterification of cellulose microfibrils and whiskers. Biomacromolecules. 2009;10(8):2144–51. doi: 10.1021/bm900319k.
- (23) Rodionova G, Hoff B, Lenes M, Eriksen Ø, Gregersen Ø. Gas-phase esterification of microfibrillated cellulose (MFC) films. Cellulose. 2013;20:1167–74. doi: 10.1007/s10570-013-9887-5.
- (24) Kim JK, Bandi R, Dadigala R, Van Hai L, Han SY, Kwon GJ, et al. Esterification of nanofibrillated cellulose using lauroyl chloride and its composite films with polybutylene succinate. Bioresources. 2023;18(4):7143–53. doi: 10.15376/biores.18.4.7143-7153.
- (25) Wei L, Agarwal UP, Hirth KC, Matuana LM, Sabo RC, Stark NM. Chemical modification of nanocellulose with canola oil fatty acid

- methyl ester. Carbohydr Polym. 2017;169:108–16. doi: 10.1016/j.carbpol.2017.04.008.
- (26) Wen X, Wang H, Wei Y, Wang X, Liu C. Preparation and characterization of cellulose laurate ester by catalyzed transesterification. Carbohydr Polym. 2017;168:247–54. doi: 10.1016/j.carbpol.2017. 03.074.
- (27) Fumagalli M, Ouhab D, Boisseau SM, Heux L. Versatile gas-phase reactions for surface to bulk esterification of cellulose microfibrils aerogels. Biomacromolecules. 2013;14(9):3246–55. doi: 10.1021/ bm400864z.
- (28) Jandura P, Kokta BV, Riedl B. Fibrous long-chain organic acid cellulose esters and their characterization by diffuse reflectance FTIR spectroscopy, solid-state CP/MAS13C-NMR, and X-ray diffraction. J Appl Polym Sci. 2000;78(7):1354–65. doi: 10.1002/1097-4628(20001114)78:7<1354: AID-APP60>3.0.CO;2-V.
- (29) Almasi H, Ghanbarzadeh B, Dehghannia J, Pirsa S, Zandi M. Heterogeneous modification of softwoods cellulose nanofibers with oleic acid: Effect of reaction time and oleic acid concentration. Fibers Polym. 2015;16:1715–22. doi: 10.1007/s12221-015-4294-1.
- (30) David G, Gontard N, Guerin D, Heux L, Lecomte J, Molina-Boisseau S, et al. Exploring the potential of gas-phase esterification to hydrophobize the surface of micrometric cellulose particles. Eur Polym J. 2019;115:138–46. doi: 10.1016/j.eurpolymj.2019.03.002.
- (31) Trinh BM, Mekonnen T. Hydrophobic esterification of cellulose nanocrystals for epoxy reinforcement. Polymer. 2018;155:64–74. doi: 10.1016/j.polymer.2018.08.076.
- (32) Guo Y, Wang X, Li D, Du H, Wang X, Sun R. Synthesis and characterization of hydrophobic long-chain fatty acylated cellulose and its self-assembled nanoparticles. Polym Bull. 2012;69(4):389–403. doi: 10.1007/s00289-012-0729-7.